Electronic Supporting Information

Green Circularly Polarized Luminescence with a High Dissymmetry Factor Emitted by a [2.2]Fluorenonophane

André Loleit[a], Lars Eckhardt[b], Markus Ströbele[c], Jonas L. Hiller[b], Marcus Scheele[b,*], Holger F. Bettinger[a,*]

[a] Institut für Organische Chemie, Universität Tübingen, Auf der Morgenstelle 18, Tübingen 72076, Germany. E-mail: holger.bettinger@uni-tuebingen.de

[b] Institut für Physikalische und Theoretische Chemie, Universität Tübingen, Auf der Morgenstelle 18, Tübingen 72076

[c] Institut für Anorganische Chemie, Universität Tübingen, Auf der Morgenstelle 18, Tübingen 72076

Table of contents

1. Materials and Synthesis

General

Unless otherwise mentioned, all experiments have been carried out under ambient conditions. All chemicals and solvents were purchased from commercial suppliers and used without further purification. TLC was done using precoated polyester sheets (40×80 mm) from Machery-Nagel (POLYGAM® SILG/UV254) with 0.2 mm silica gel 60 with fluorescent indicator. NMR spectra were recorded on a Bruker Avance III 400 or a Bruker Avance III HDX 700 spectrometer. The chemical shifts δ are reported in ppm relative to the solvent signal.[1] High resolution electrospray ionization (HR-ESI) mass spectra were recorded on a maXis-4G-spectrometer from Bruker Daltonics with a time-of-flight mass detector. Absorption spectra have been measured at rt on a Lambda 1050 spectrometer from PerkinElmer with a PerkinElmer 3D WB Det module. Fluorescence spectra were measured on the same spectrometer setup as the CPL spectra with the quarter wave plate set to 0° relative to the linear polarizer (for a detailed description of the setup, see chapter 5). Fluorescence lifetime measurements were performed using time-correlated single photon counting (TCSPC). The excitation light was provided by a 405 nm PicoQuant LDH-P-C-405 diode laser pulsed at 10 MHz. The laser beam was focused into a 2 mm Hellma quartz macro cuvette containing the sample solution. Emission light was collected in 90° geometry after passing through a Semrock EdgeBasic 405 nm long-pass filter to remove excitation light. Fluorescence was detected with a PicoQuant PDM-series single-photon avalanche diode (SPAD; 100 µm active area), connected to a HydraHarp 400 TCSPC module. Data acquisition and analysis were carried out using the PicoQuant SymPhoTime64 software. Instrument response functions (IRFs) were recorded using the corresponding pure solvent under identical conditions, without the long-pass filter. ECD spectra were recorded with a Jasco J-1500 spectropolarimeter in dichloromethane solution. Absolute fluorescence quantum yield was measured on a PerkinElmer FL 8500 Spectrophotometer

equipped with a 150 W continuous Xe short arc lamp as excitation source and an integration sphere. All spectra were baseline corrected. All measurements were done in HPLC grade solvents. Specific rotations ($[\alpha]_D^{20}$) were measured with a Polarimeter 341 from Perkin-Elmer.

Materials

Enantiopure forms of ***(R$_p$)-/(S$_p$)-2*** were prepared according to the literature.[2] The *pseudo-meta*-dibromo[2.2]paracyclophane required for the synthesis of ***(R$_p$)-/(S$_p$)-2*** was purchased from abcr GmbH and used without further purification.

Synthesis Procedures

(*R$_p$*)-/(*S$_p$*)-3

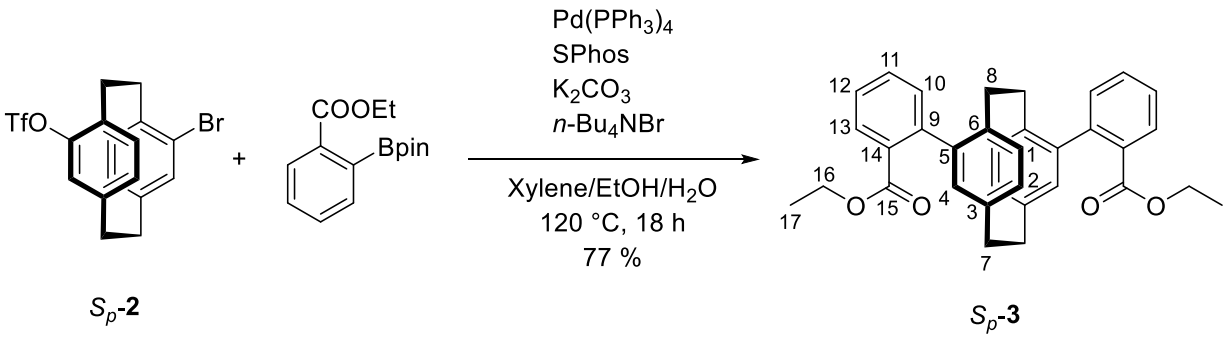

S$_p$-**2** *S$_p$*-**3**

A modified version of the literature procedure was used to synthesize ***(S$_p$)-3***.[3] In a pressure tube ***(S$_p$)-2*** (160 mg, 0.366 mmol, 1.00 eq.), ethyl 2-(4,4,5,5-tetramethyl-1,3,2-dioxaborolan-2-yl)benzoate (303 mg, 1.10 mmol, 3.00 eq.), $Pd(PPh_3)_4$ (84.6 mg, 73,2 µmol, 0.20 eq.), SPhos (30.1 mg, 73.2 µmol, 0.20 eq.), K_2CO_3 (304 mg, 2.20 µmol, 0.20 eq.) and tetrabutylammonium bromide (241 mg, 0.732 mmol, 2.00 eq.) were dissolved in a mixture of xylene (isomeric mixture)/EtOH/H_2O (4 mL, 2/1/1 v/v/v). The reaction mixture was purged with Ar for 15 min.

The sealed tube was stirred at 120 °C for 18 h. The reaction mixture was diluted with water and extracted with dichloromethane. The organic phase was dried over Na_2SO_4. The solvent was removed under reduced pressure. The crude product was purified by silica gel chromatography (*n*-hexane/ethyl acetate 10:1, R_f = 0.16). ***(S$_p$)*-3** was obtained as a colorless crystalline powder (142 mg, 0.282 mmol, 77 %).

***(R$_p$)*-3** was obtained by the same procedure starting from ***(R$_p$)*-2**.

^{1}H NMR (CD_2Cl_2, 400 MHz) δ [ppm]: 7.79 (dd, ^{3}J = 7.7 Hz, ^{4}J = 1.0 Hz, 2H, H-13), 7.71 (vtd, ^{3}J = 7.7 Hz, ^{4}J = 1.4 Hz, 2H, H-12), 7.65 (dd, ^{3}J = 7.7 Hz, ^{4}J = 1.4 Hz, 2H, H-10), 7.45 (vtd, ^{3}J = 7.7 Hz, ^{4}J = 1.0 Hz, 2H, H-11), 6.74 (d, ^{4}J = 1.9 Hz, 2H, H-4), 6.55 (dd, ^{3}J = 7.8 Hz, ^{4}J = 1.9 Hz, 2H, H-2), 6.46 (d, ^{3}J = 7.8 Hz, 2H, H-1), 3.97-3.81 (m, 4H, H-16), 3.28-3.09 (m, 4H, H-7a/7b), 2.62-2.47 (m, 4H, H-8a/8b), 0.88 (d, ^{3}J = 7.1 Hz, 6H, H-17).

^{13}C{^{1}H} NMR (CD_2Cl_2, 101 MHz) δ [ppm]: 169.4 (C-15), 140.9 (C-14), 140.7 (C-5), 139.8 (C-3), 138.8 (C-6), 134.5 (C-9), 132.6 (C-2), 131.6 (C-4 or C-12), 131.6 (C-4 or C-12), 131.5 (C-1), 130.8 (C-13), 129.2 (C-11), 127.4 (C-10), 61.2 (C-16), 35.4 (C-7), 33.2 (C-8), 13.9 (C-17).

HR-ESI-MS: calcd. For $C_{34}H_{32}O_4Na$ $[M+Na]^+$: 527.21928, found: 527.21950 m/z (Δ: -0.42 ppm).

***(R_p)-/(S_p)*-1**

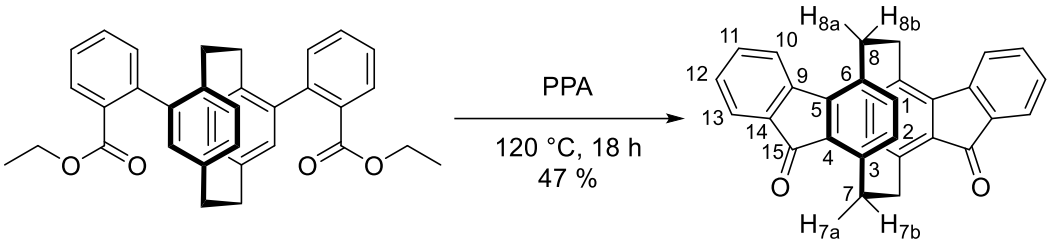

(S_p)-**3** *(R_p)*-**1**

Compound ***(R_p)*-1** was synthesized according to a literature procedure.[3] ***(S_p)*-3** (180 mg, 0.361 mmol, 1.00 eq.) was stirred in polyphosphoric acid (10 mL) at 120 °C for 18 h. The reaction mixture was diluted with water and extracted with ethyl acetate. The organic phase was dried over Na_2SO_4. The solvent was removed under reduced pressure. The crude product was purified by silica gel chromatography (*n*-hexane/ethyl acetate 5:1, R_f = 0.28). ***(R_p)*-1** was obtained as a yellow powder (70.0 mg, 0.170 mmol, 47 %). $[\alpha]_{589}^{20}$ = +1522 ° (c = 0.10, $CDCl_3$)

***(S_p)*-1** was obtained by the same procedure starting from ***(R_p)*-3**. $[\alpha]_{589}^{20}$ = -1534 ° (c = 0.10, $CDCl_3$)

^{1}H NMR (CD_2Cl_2, 700 MHz) δ [ppm]: 7.68-7.64 (m, 4H, H-10 + H-13), 7.57 (vtd, ^3J = 7.4 Hz, ^4J = 1.2 Hz, 2H, H-11 or H-12), 7.34 (vtd, ^3J = 7.4 Hz, ^4J = 1.2 Hz, 2H, H-11 or H-12), 6.22 (s, 4H, H-1 + H-2), 4.13-4.08 (m, 2 H, H-7a), 3.78-3.72 (m, 2 H, H-8a), 3.08-3.02 (m, 2 H, H-8b), 2.94-2.88 (m, 2 H, H-7b).

^{13}C{^{1}H} NMR (CD_2Cl_2, 176 MHz) δ [ppm]: 194.6 (C-15), 146.5 (C-6), 145.1 (C-14 or C-9), 142.2 (C-4), 137.2 (C-1), 136.0 (C-5), 135.2 (C-14 or C-9), 135.1 (C-11 or C-12), 135.0 (C-3), 133.0 (C-2), 129.0 (C-11 or C-12), 124.4 (C-10 or C-13), 123.6 (C-10 or C-13), 31.8 (C-8), 30.0 (C-7).

HR-ESI-MS: calcd. for $C_{30}H_{20}O_2Na$ $[M+Na]^+$: 435.13555, found: 435.13502 m/z (Δ: 1.21 ppm).

2. NMR and MS spectra

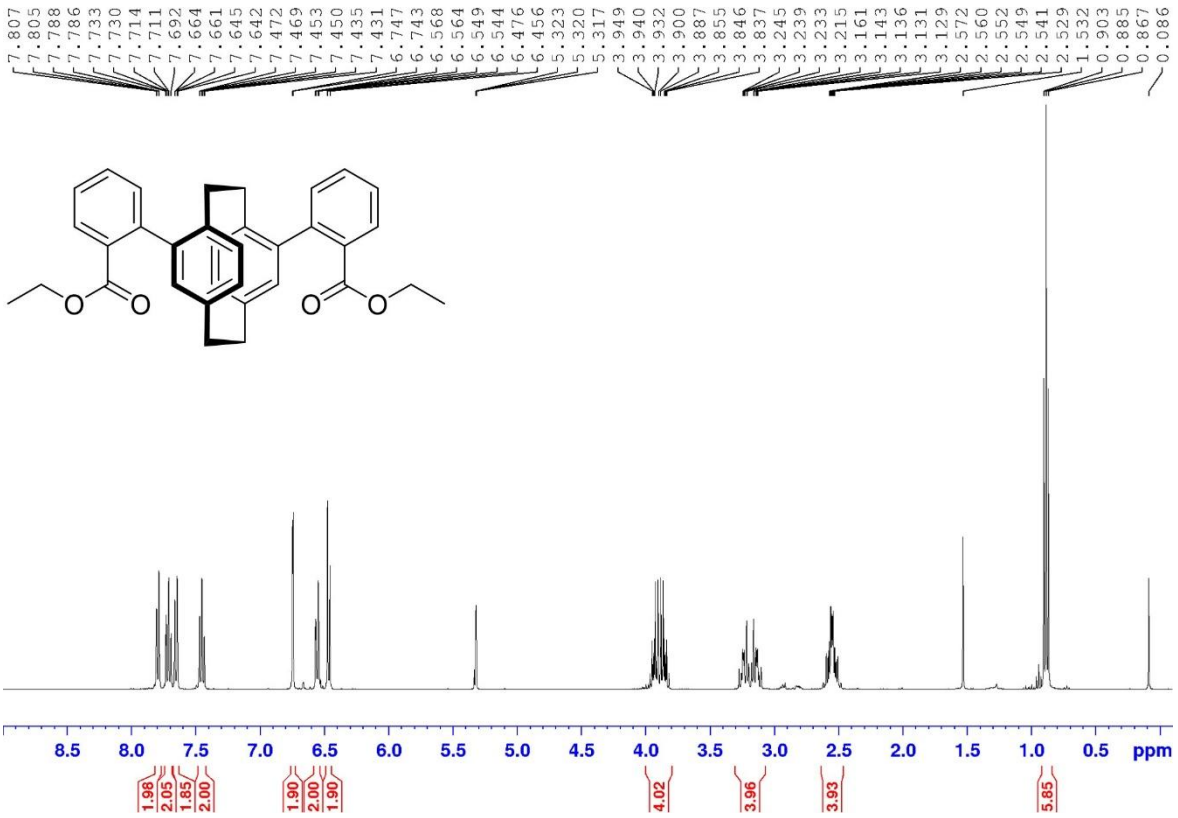

Figure S1: ^{1}H NMR (CD_2Cl_2, 400 MHz) of **3**.

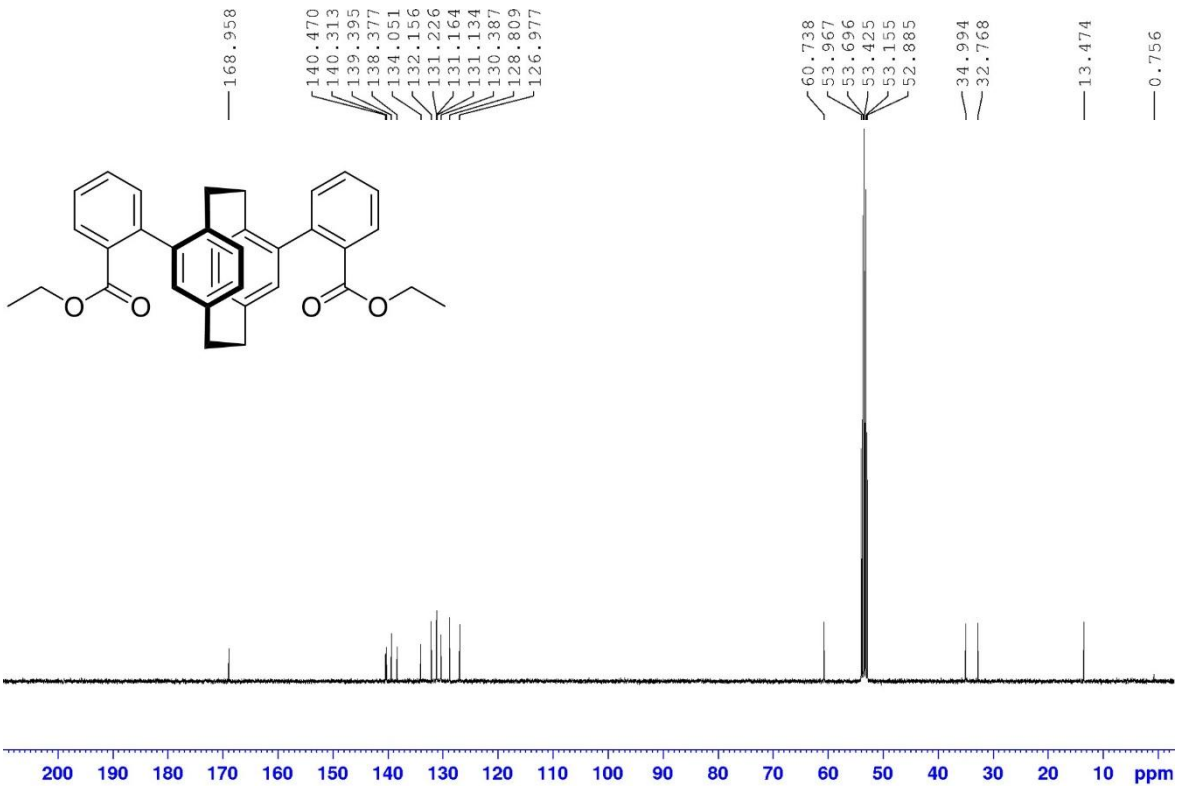

Figure S2: ^{13}C NMR (CD_2Cl_2, 101 MHz) of **3**.

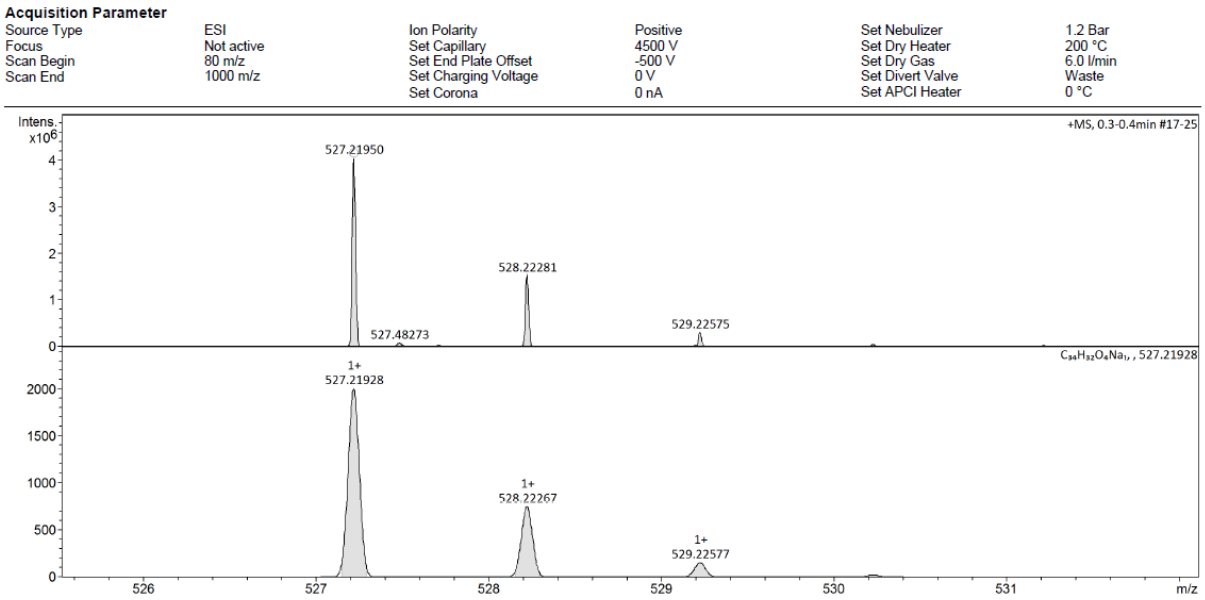

Figure S3: Experimental HR-ESI-MS of **3** (top) and theoretical isotopic envelopes for $C_{34}H_{32}O_4Na$ $[M+Na]^+$ (bottom). m/z $[M+Na]^+$ calculated for $C_{30}H_{20}O_2Na$: 527.21928; found: 527.21950 m/z (Δ: -0.42 ppm).

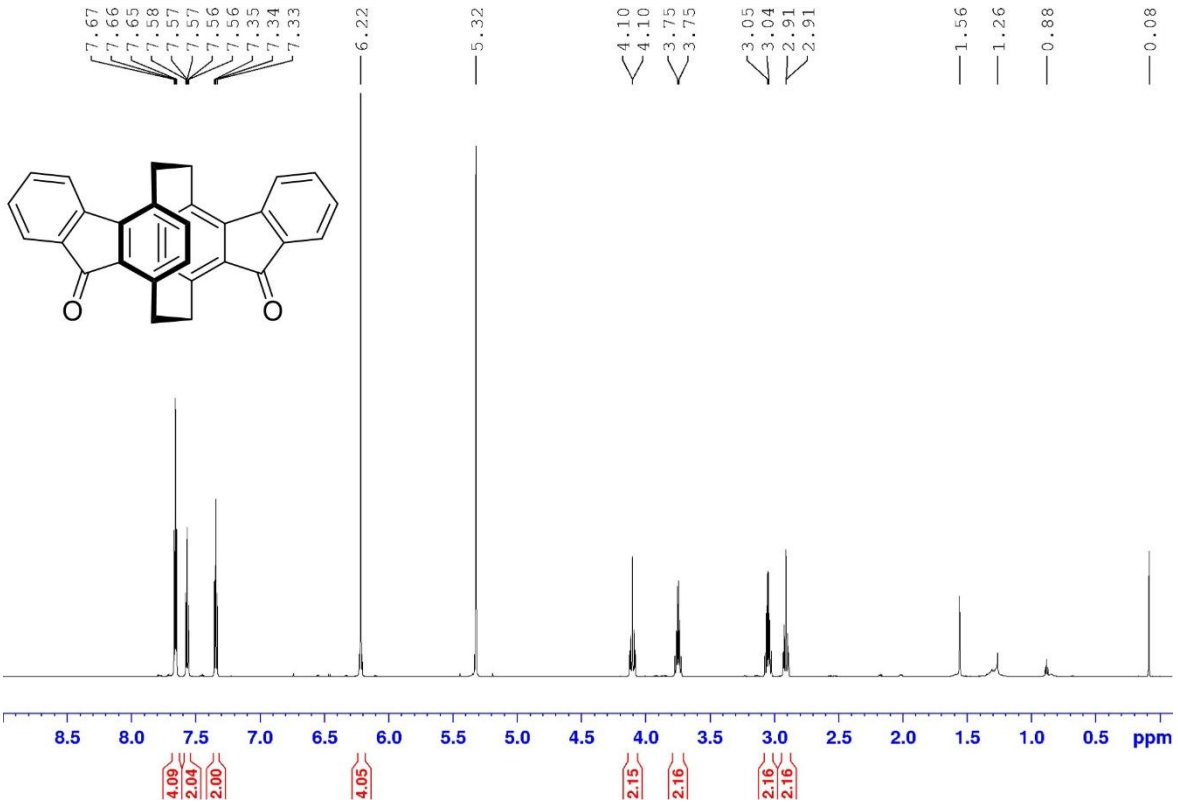

Figure S4: ^1H NMR (CD_2Cl_2, 700 MHz) of **1**.

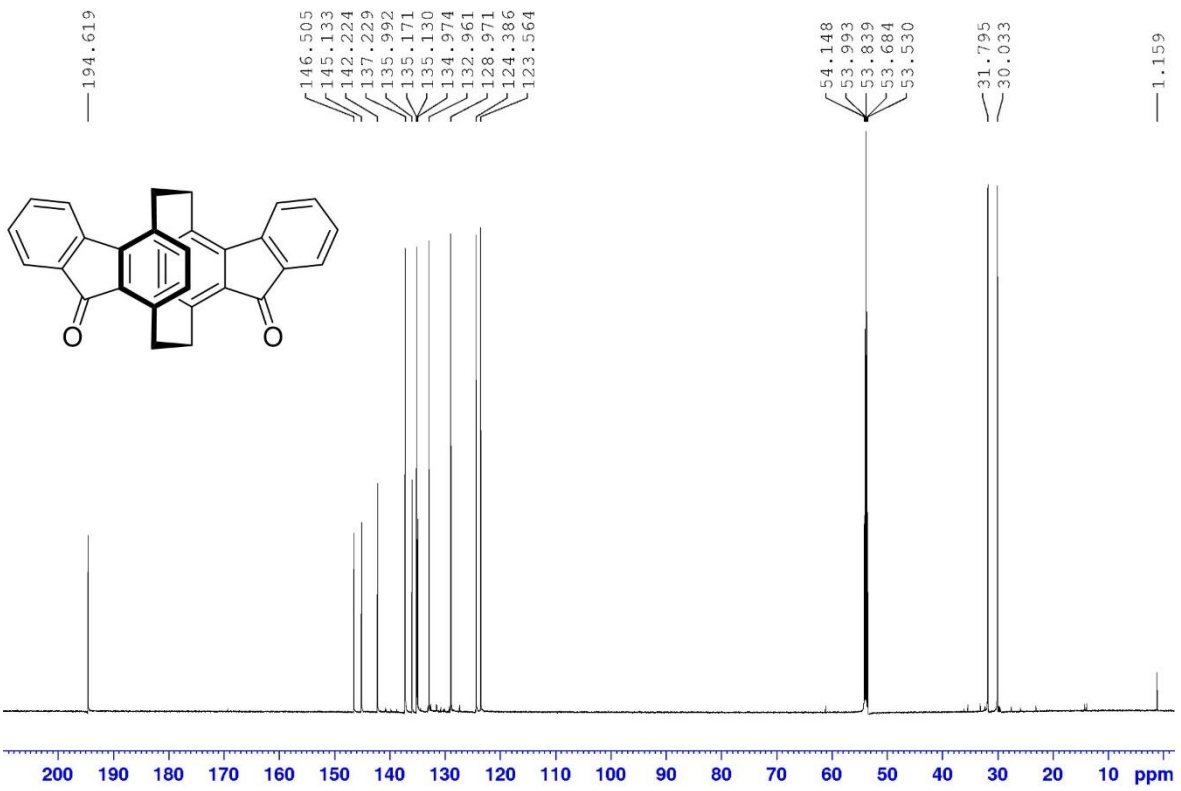

Figure S5: ^{13}C NMR (CD_2Cl_2, 176 MHz) of **1**.

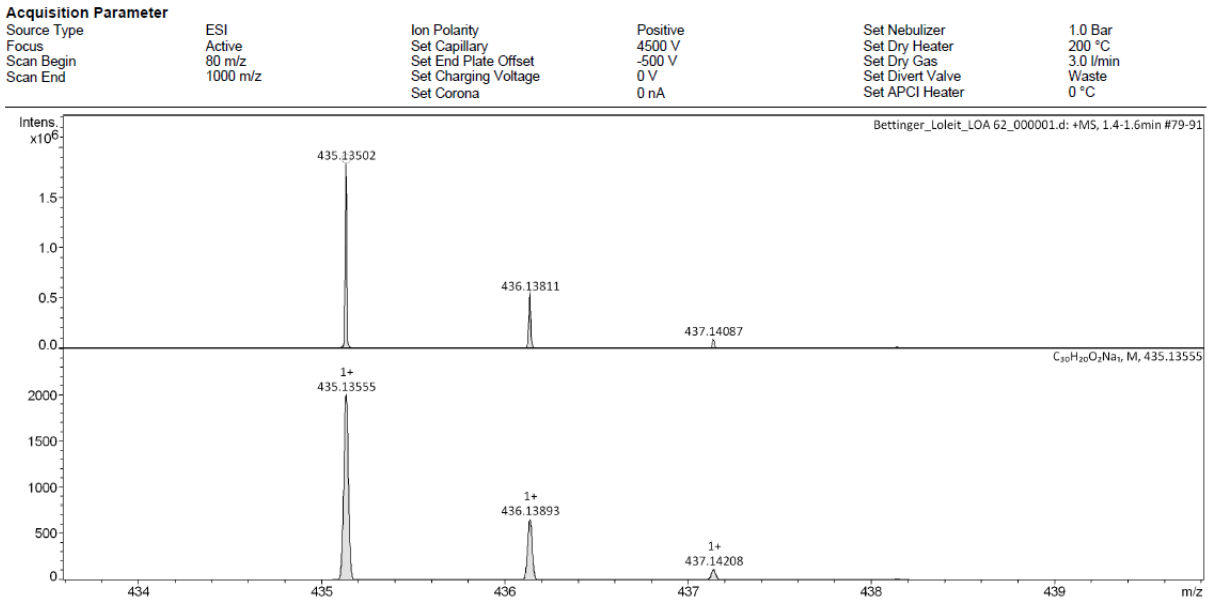

Figure S6: Experimental HR-ESI-MS of **1** (top) and theoretical isotopic envelopes for $C_{30}H_{20}O_2Na$ $[M+Na]^+$ (bottom). m/z $[M+Na]^+$ calculated for $C_{30}H_{20}O_2Na$: 435.13555; found: 435.13502 (Δ: 1.21 ppm).

3. HPLC

As an indirect proof of the enantiopurity of the starting material ***(R*$_p$*)-/(S*$_p$*)*-2** a HPLC analysis of the diastereomeric camphanic esters, which are the key intermediates in the optical resolution process of Morisaki *et al.*,[2] was performed.

HPLC conditions:

Column: CHIRALPAK IG 4.6 mmI.D. x 250 mmL, Particle Size: 5 µm

Eluent: n-Hexane/i-PrOH 4/1 (v/v)

Column Flow: 1.0 mL/min

λ (Detector): 254 nm

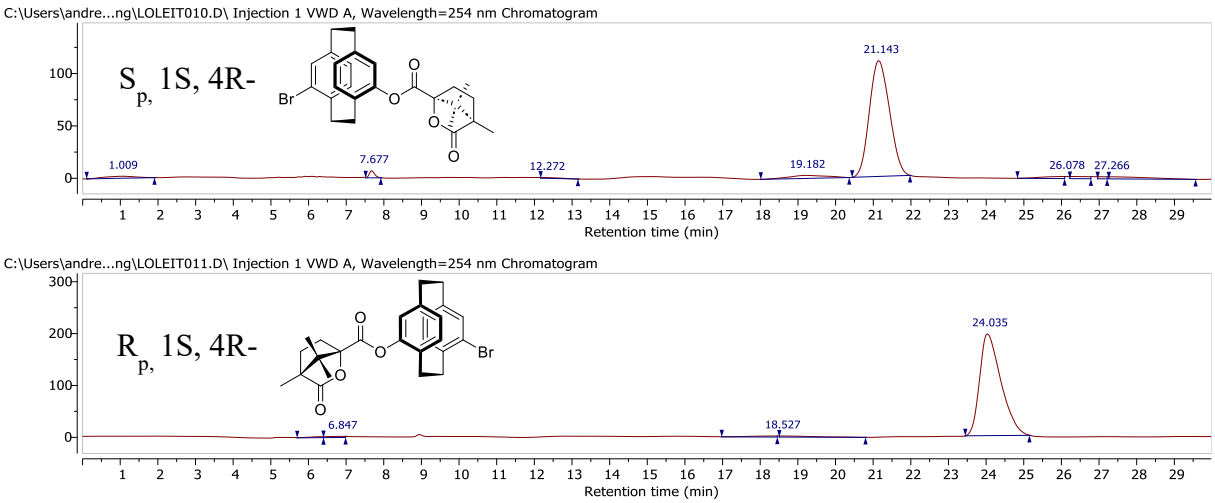

Figure S7: Chromatograms of the diastereomers after the optical resolution.

4. Single-crystal X-ray crystallography

Single crystals of ***(R*$_P$*)*-1** suitable for X-ray crystallography were grown at 5 °C from a solution in a dichloromethane/*n*-hexane mixture. A clear colorless block-shaped crystal with dimensions 0.22 × 0.20 × 0.15 mm^3 was mounted. Data were collected using a XtaLAB Synergy, Dualflex, HyPix diffractometer operating at T = 150.00(10) K.

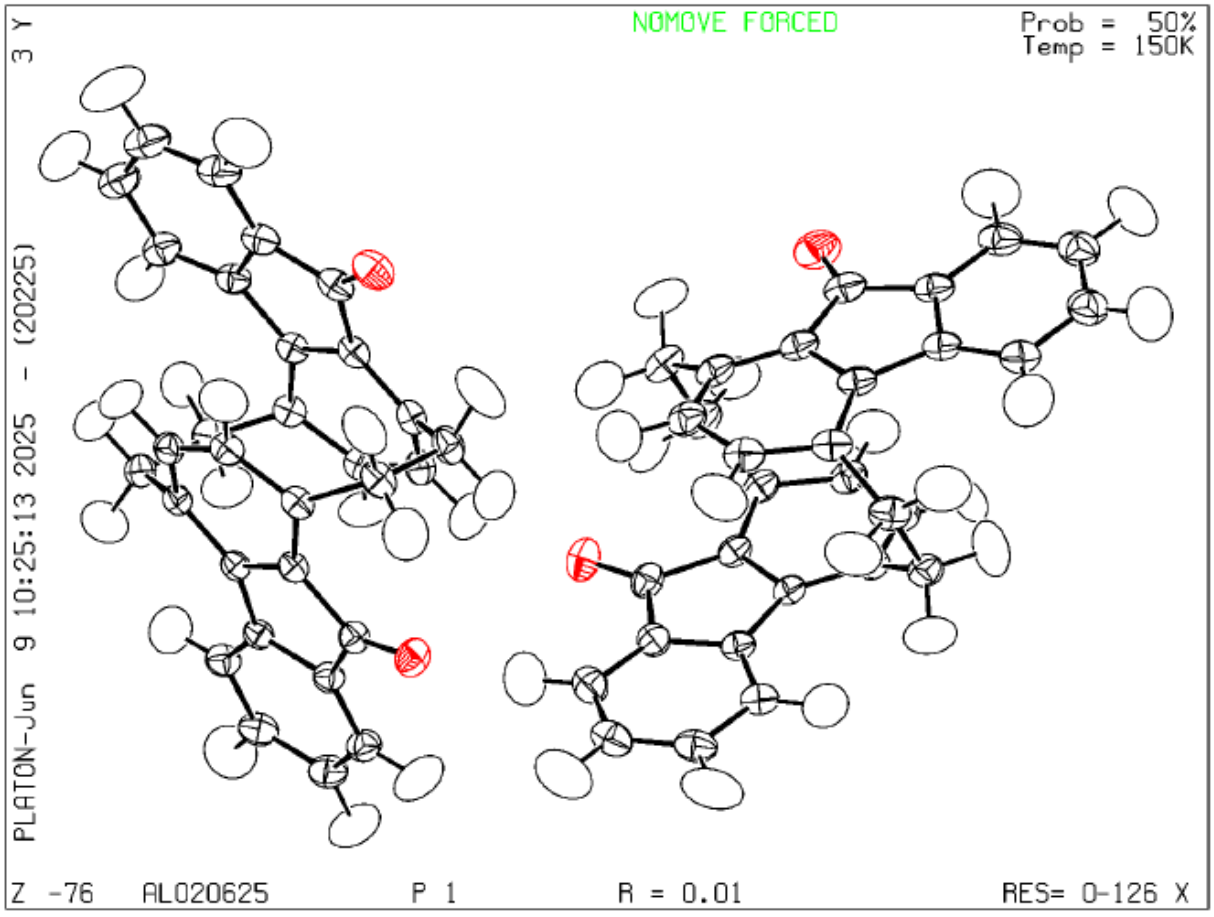

Formula	C60H40O4
CCDC	2457695
Dcalc./ g cm-3	1.360
μ/mm-1	0.659
Formula Weight	824.984
Colour	clear colourless
Shape	block-shaped
Size/mm3	0.22×0.20×0.15
T/K	150.00(10)

Crystal System	triclinic
Flack Parameter	0.02(3)
Hooft Parameter	0.02(3)
Space Group	P1
a/Å	8.8766(2)
b/Å	9.0804(2)
c/Å	14.7689(3)
a/°	73.291(2)
b/°	75.659(2)
g/°	63.147(2)
V/Å3	1007.50(4)
Z	1
Z'	1
Wavelength/Å	1.54184
Radiation type	Cu Ka
Qmin/°	3.15
Qmax/°	79.91
Measured Refl's.	41856
Indep't Refl's	8315
Refl's I≥2 s(I)	8241
Rint	0.0165
Parameters	938
Restraints	3
Largest Peak	0.1462
Deepest Hole	-0.0670
GooF	1.3208
wR2 (all data)	0.0377
wR2	0.0377
R1 (all data)	0.0143
R1	0.0142

5. Optical spectra

Solvatochromism

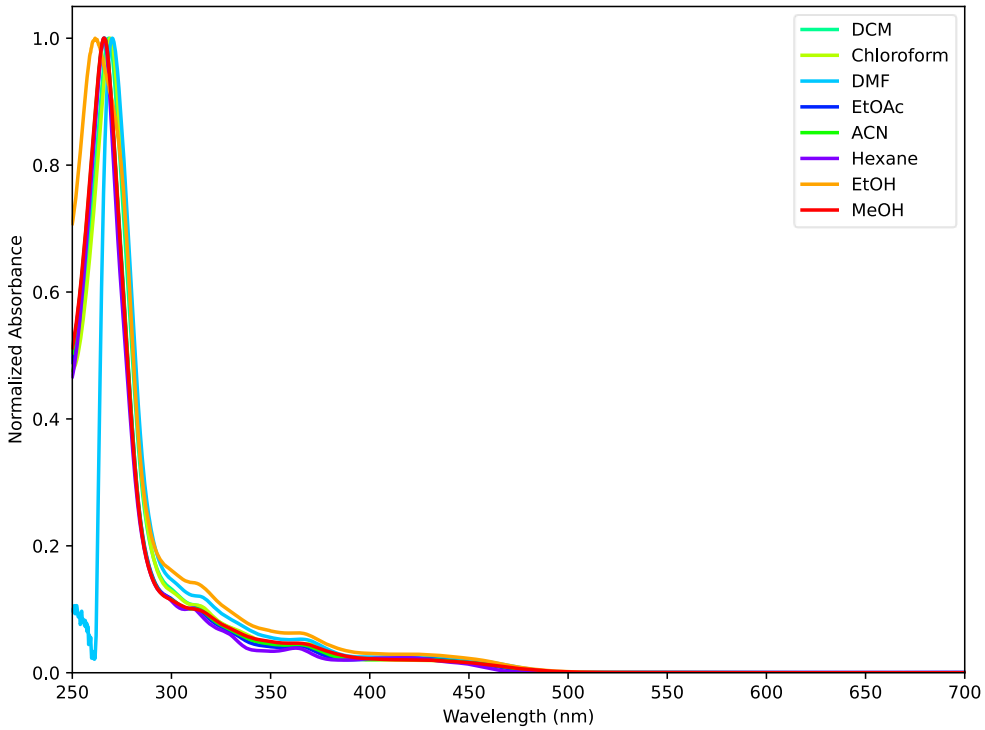

Figure S8: Normalized absorption spectra of **1** in different solvents.

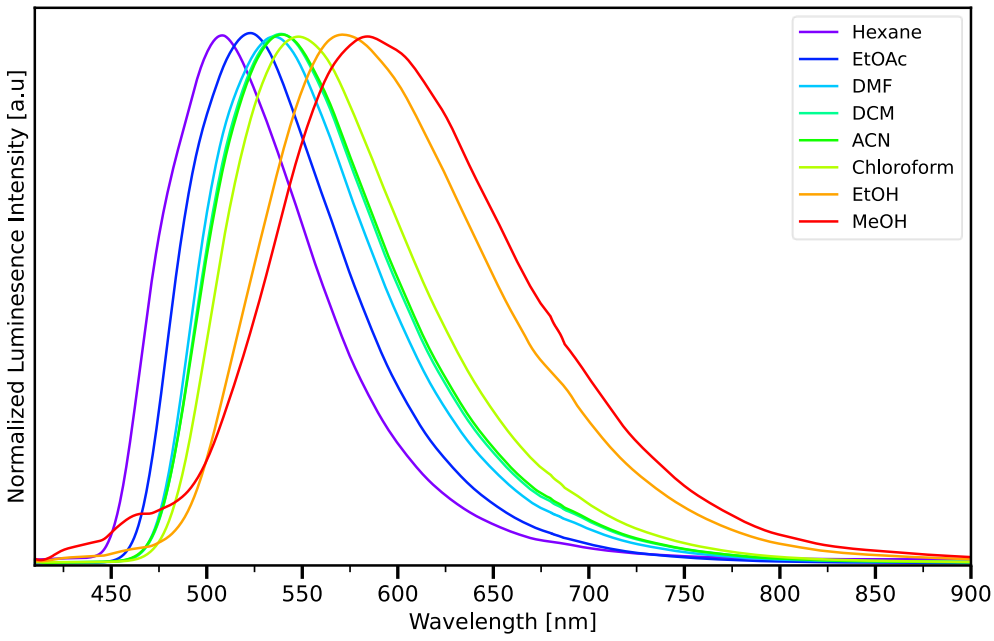

Figure S9: Normalized emission spectra of **1** in different solvents.

Lifetime

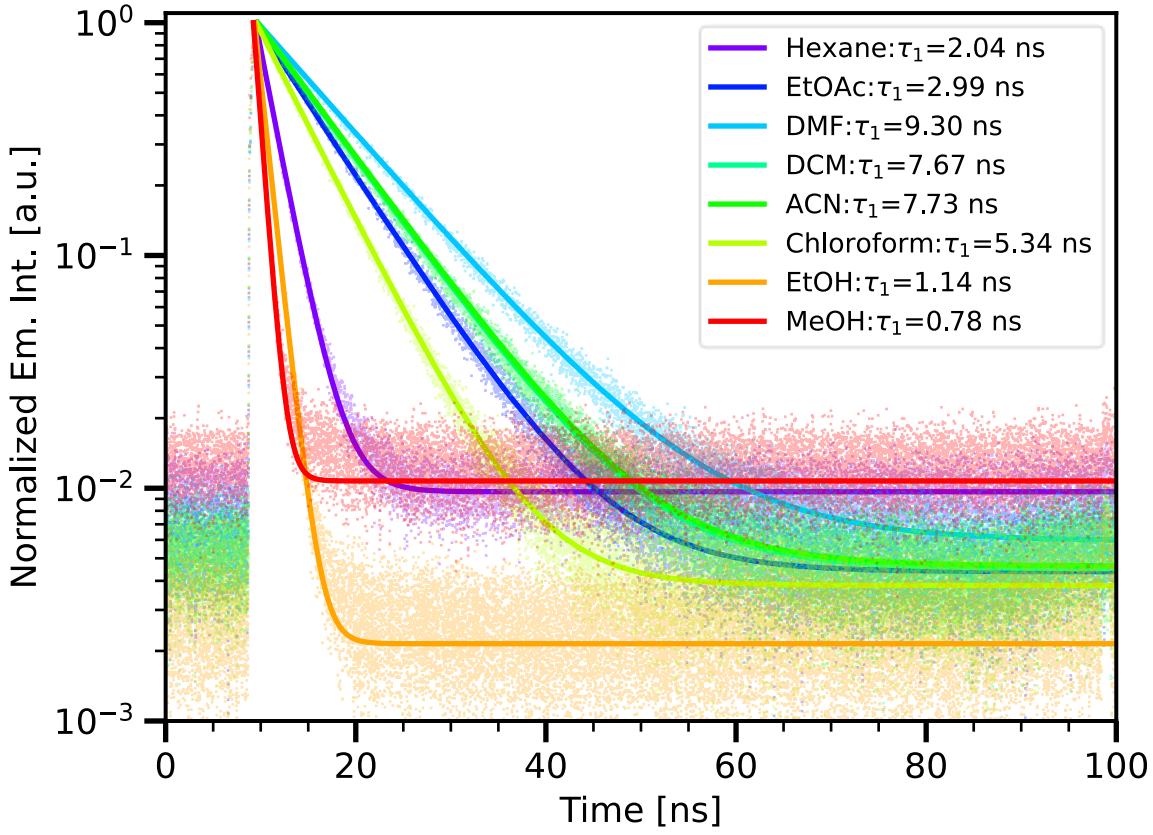

Figure S10: Photoluminescence decay of **1** in different solvents. The lifetimes were obtained by a mono exponential fit of the decay curves.

Table 1: Optical properties of **1** in different solvents. [a] Absorption maximum. [b] Emission maximum, excited at $\lambda_{ex.}$ = 405 nm. [c] Photoluminescence lifetime. [d] χ^2 of the mono exponential fit.

Solvent	**$\lambda_{abs.,max}$ [a] [nm]**	**$\lambda_{em.,max}$ [b] [nm]**	**τ_1 [c] [ns]**	**χ^2 [d]**
n-Hexane	266	509	2.04	1.13
Ethyl acetate	266	526	2.99	1.08
Dimethylformamide	270	531	9.30	1.12
Dichloromethane	268	540	7.67	1.07
Acetonitrile	266	541	7.73	1.07
Chloroform	269	548	5.34	1.02
Ethanol	262	569	1.14	1.37
Methanol	266	584	0.78	1.15

Lippert-Mataga Plot

The difference between the ground and excited state dipole moment was determined according to Lippert and Mataga by plotting the Stokes shift versus the Onsager solvent parameter and utilizing the following equation:[4,5]

$$\Delta\mu = \sqrt{\frac{\Delta\nu}{\Delta f} \cdot 2\pi\varepsilon_0 hca_0^3} = 2.70 \cdot 10^{-29}\text{Cm} = 8.09\ \text{D}$$

with:

$$\Delta f = \left(\frac{\varepsilon - 1}{2\epsilon + 1} - \frac{n^2 - 1}{2n^2 + 1}\right)$$

The Onsager cavity radius a_0 = 5.83 Å was obtained from a molecular volume calculation at the MN15/def2-TZVP level of theory with *Gaussian* 16.

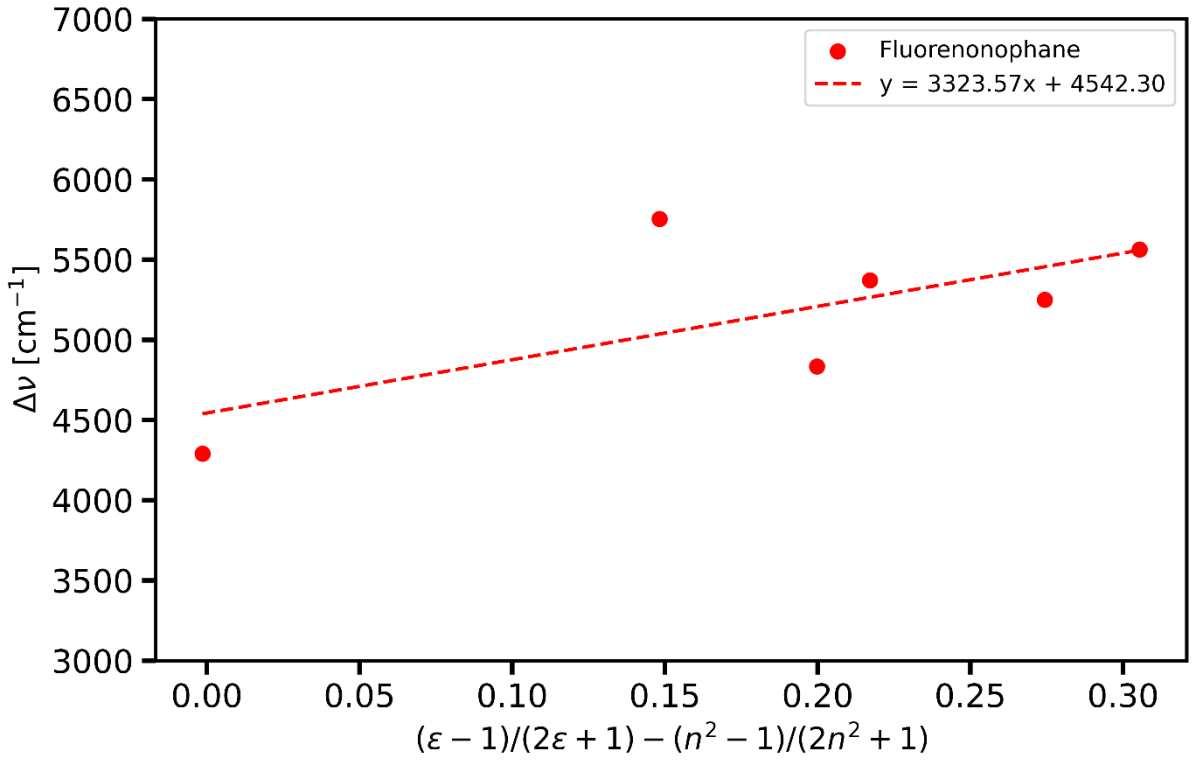

Figure S11: Lippert-Mataga plot for **1**. The solvents are (from left to right) n-hexane, chloroform, ethyl acetate, DCM, dimethylformamide, acetonitrile. R^2 of the fit is 0.46.

CPL

CPL is recorded on the home-built setup shown in Figure S12.

The excitation source is a 405 nm PicoQuant LDH-P-C-405 diode laser, which is linearly, vertically polarized and operated in continuous wave mode. The laser is controlled by a PicoQuant PDL 800-D laser driver. The laser beam is first expanded and spatially filtered using a pinhole aperture, allowing only the central Gaussian profile of the intensity to pass through. To eliminate unwanted signals from secondary laser emissions, a 405/10 nm bandpass laser line filter (Semrock BrightLine FF01-405/10-25) is positioned in the excitation path. For some measurements an additional optical density filter was added at this position to reduce illumination intensity on the sample with the magnitude selected depending on the sample. The filtered light is then focused onto a 2 mm quartz glass cuvette containing the sample solution.

Fluorescence is collected in a 180° geometry. The emission is collimated and passed through a rotatable achromatic quarter-wave plate (Thorlabs AQWP05M-600), which converts circular polarized into linear polarized light, which is then filtered out using a thin-film linear polarizer (Thorlabs LPVISE100-A). The thin-film polarizer is fixed at a horizontal position, which removes most of the vertically polarizer excitation light. To remove residual excitation light, a long-pass filter (458 nm for standard measurements, 405 nm for measurements below 458 nm and 405+458 nm for IR measurements) is placed after the linear polarizer.

Spectral data is collected using an Andor Shamrock 303i-B spectrograph. It employs a grating to separate the light according to its wavelength and detects with an Andor iDus 401A-BVF CCD camera, which is cooled to -60°C. There are three different gratings: 150 grooves/mm, 300 grooves/mm and 1200 grooves/mm. Before each measurement, the signal light beam is focused onto the center of the camera. Entrance slit width, integration time and grating were selected depending on the sample.

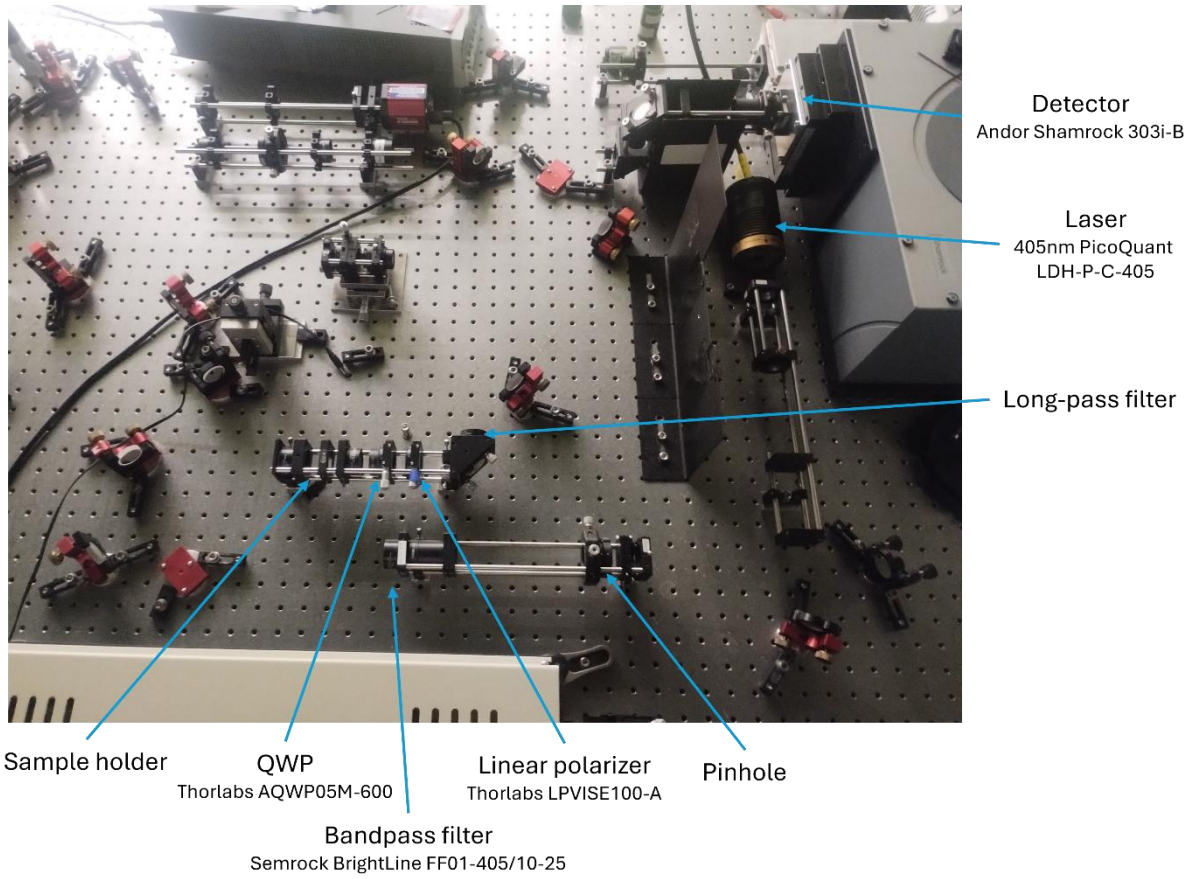

Figure S12: Photograph of the employed setup with labelling of the relevant components.

To acquire CPL spectra, two emission spectra are recorded: once with the QWP set to +45° and once to -45° relative to the linear polarizer. The order of the two measurements is altered to rule out degradation of the signal for example by photobleaching or precipitation. The two QWP settings result in the intensities of left- and right-handed CPL (I_L and I_R), which are then normalized and subtracted to generate the final ΔI spectrum. The luminescence dissymmetry factor, g_{lum}, is subsequently calculated across the full spectral range using equation $g_{lum}=2\,\Delta I(\lambda)/I(\lambda)$, where $\Delta I(\lambda)=I_L(\lambda)-I_R(\lambda)$ and $I(\lambda)=I_L(\lambda)+I_R(\lambda)$. A linear fit is applied to avoid choosing a noise spike as g_{lum} maximum.

The functionality of the spectrometer was verified using the Eu:BPEPC analogue Eu-tris-(4-((4-methoxyphenyl)ethynyl)-N,N'-bis(1-phenylethyl)-pyridine-2,6-dicarboxamide) (short

Eu(L)3), which was proposed by Starck et al. as a reference complex for CPL.[6] The recorded spectra exhibit mirror-symmetric CPL features at 590, 595, 616, 620, 649, 651, 695 and 704 nm (see Figure S11 and S12), which are in agreement in terms of position and magnitude of g_{lum} with the results published in the literature.[6]

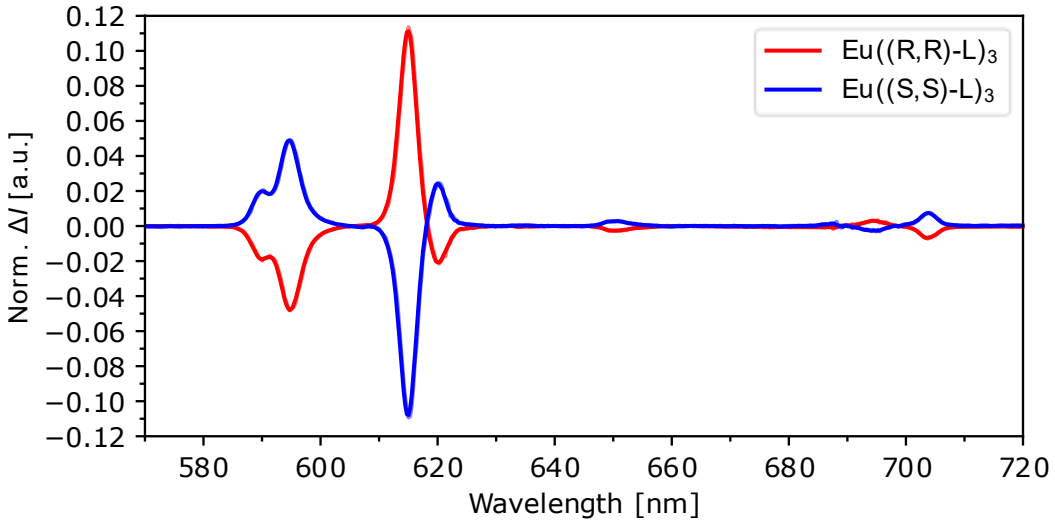

Figure S13: CPL spectrum of $Eu(L)_3$.

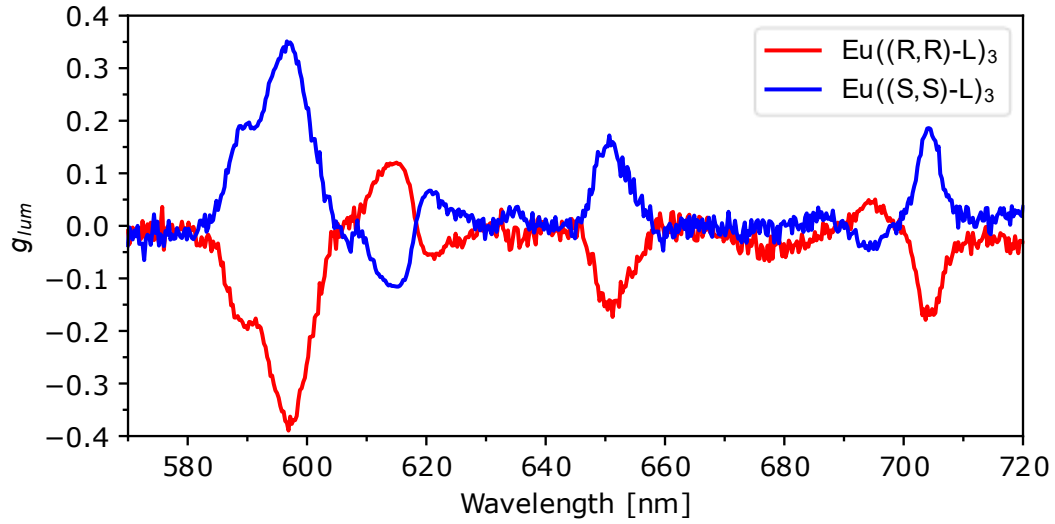

Figure S14: g_{lum} vs. wavelength plot of $Eu(L)_3$.

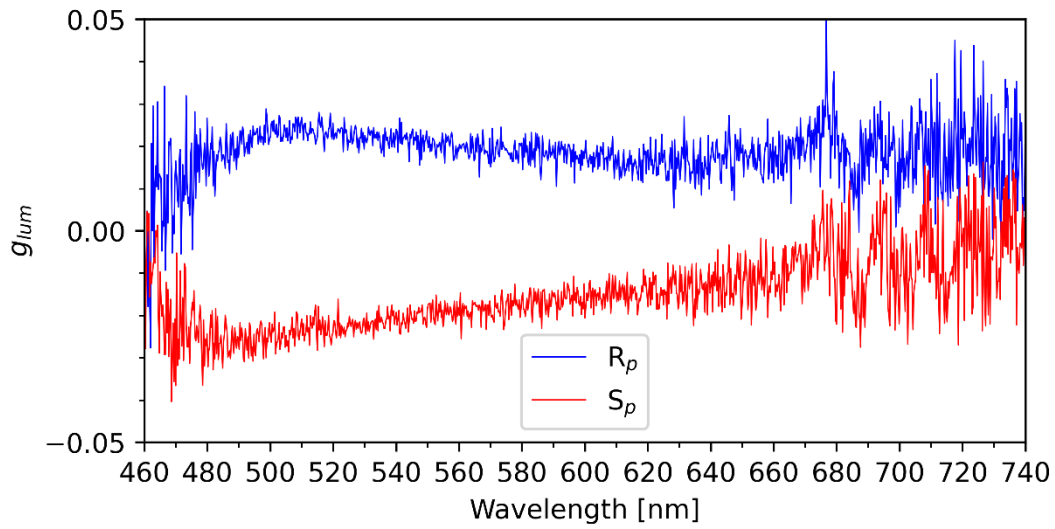

Figure S15: g_{lum} vs. wavelength plot of **1**.

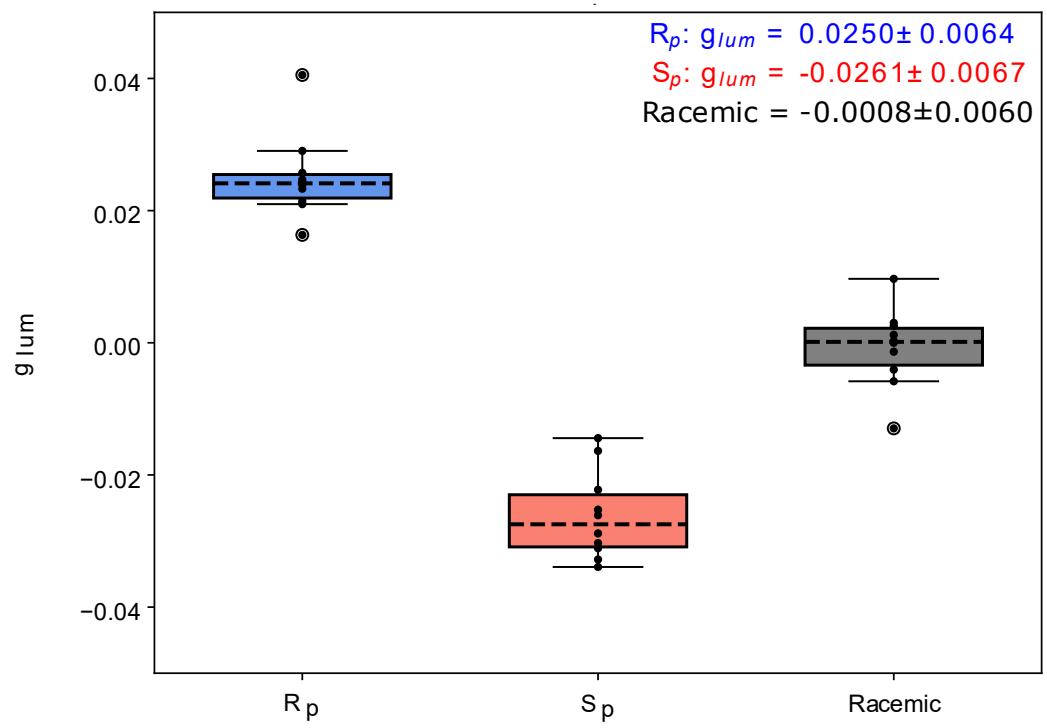

Figure S16: Box plots of the determined g_{lum} factors from CPL measurements for R_p-**1** (blue), S_p-**1** (red) and the racemic mixture of **1** (black) in dichloromethane solution.

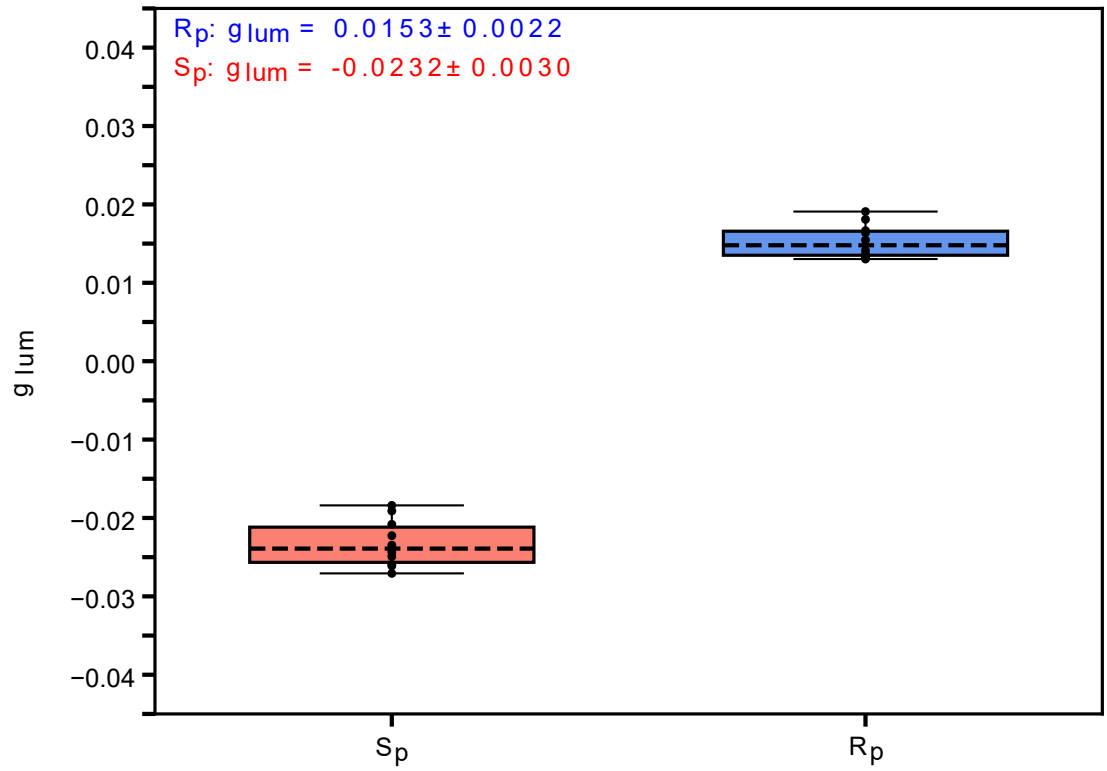

Figure S17: Box plots of the determined glum factors from CPL measurements for *(Sp)*-**1** (blue), *(Rp)*-**1** (red) in acetonitrile solution.

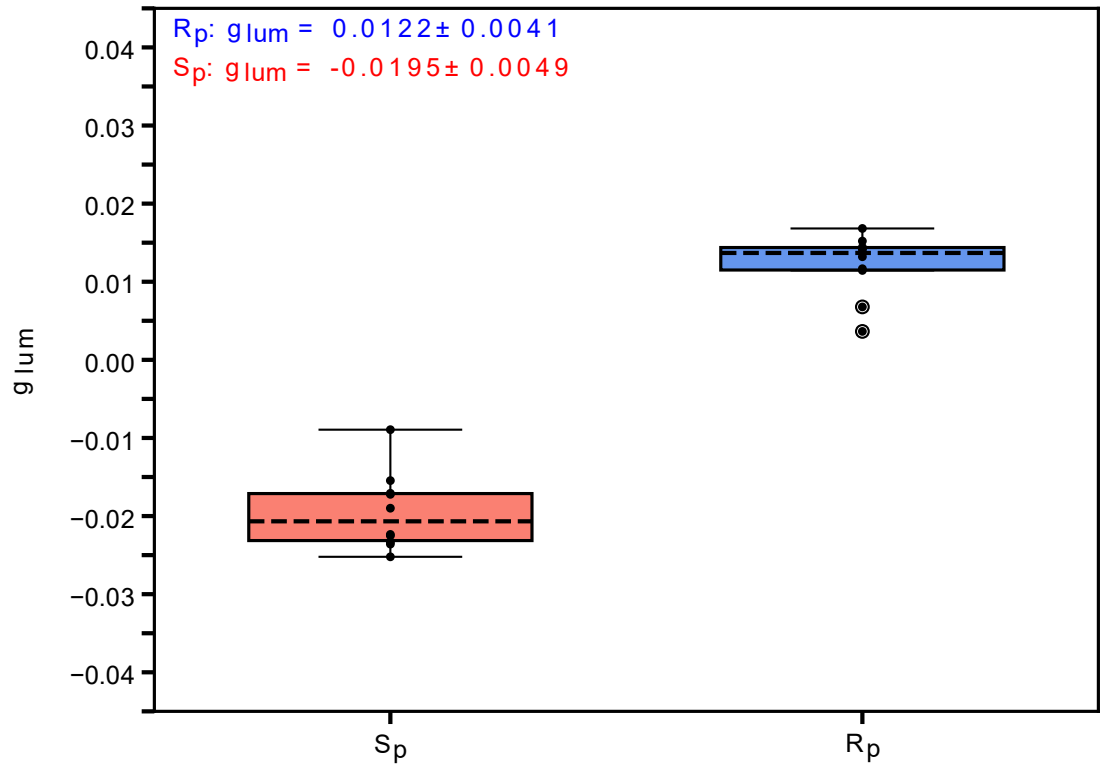

Figure S18: Box plots of the determined g_{lum} factors from CPL measurements for *(Sp)*-**1** (blue), *(Rp)*-**1** (red) in hexane solution.

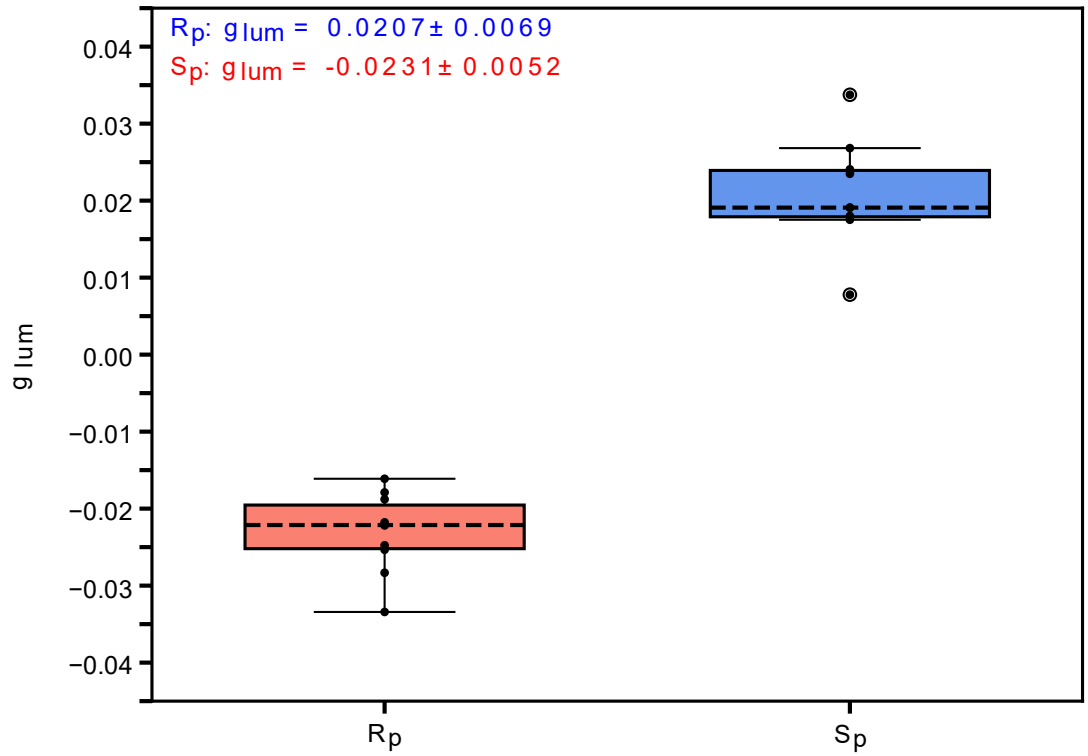

Figure S19: Box plots of the determined glum factors from CPL measurements for *(Sp)*-**1** (blue), *(Rp)*-**1** (red) in ethanol solution.

6. Computational studies

All computations were performed with the *Gaussian* 16 program.[7] Ground state geometry optimizations were done using the MN15 functional[8] in conjunction with the def2-TZVP basis set.[9] The optimized ground state geometries were subjected to the optimization of the excited state geometries and to TD-DFT single point calculations both at the TD-MN15/def2-TZVP level of theory.[8–19] For an accurate computational reproduction of the absorption spectrum solvent effects were taken into account, the corresponding calculations were performed using the continuum solvation model SMD.[20] Without a solvation model the single point TD-DFT calculations predict a nπ*- instead of a ππ*-character for the S_1 state. This behavior is similar to studies of 9-fluorenone, where computational and experimental studies suggest a ππ*-

character for the S1 state in polar solutions, while vacuum calculations predict a nπ*-character.[21–23]

Optical spectra (Absorption and ECD)

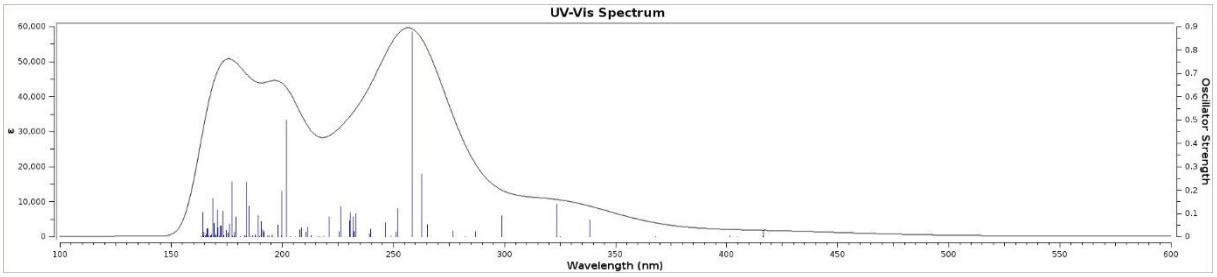

Figure S20: Absorption spectrum of *(R_p)*-**1** including the first 100 excited states computed at the TD-MN15/def2-TZVP/SMD(CH_2Cl_2) level of theory.

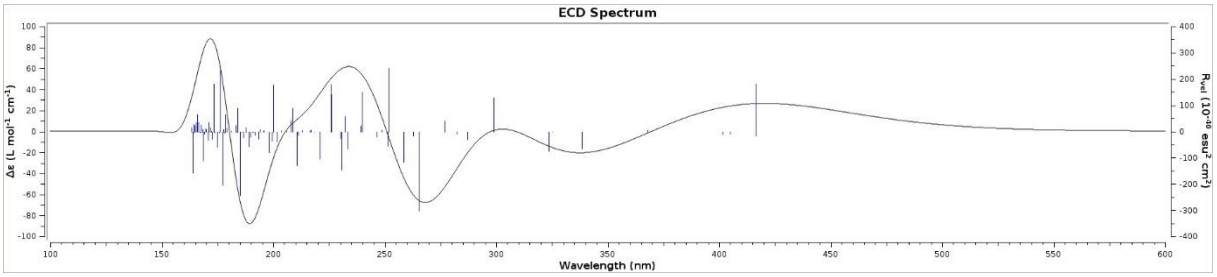

Figure S21: ECD spectrum of *(R_p)*-**1** including the first 100 excited states computed at the TD-MN15/def2-TZVP/SMD(CH_2Cl_2) level of theory.

Natural transition orbitals for the absorption

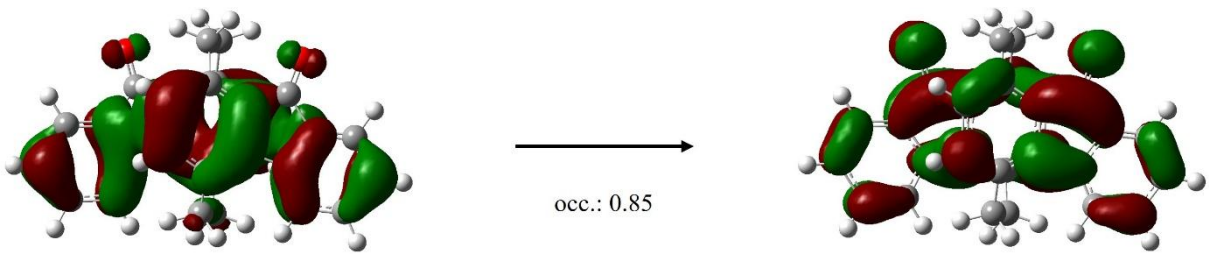

Figure S22: Dominant NTO pair for the $S_0 \rightarrow S_1$ absorption of **1** with its relative contribution calculated at the MN15/def2-TZVP/SMD(CH_2Cl_2) level of theory.

Dissymmetry factor $g_{lum,calcd.}$

The dissymmetry factor $g_{lum,calcd.}$ was calculated according to the equation g = 4R/(D+G). R is defined as the scalar product of electric ($\vec{\mu}$) and magnetic ($\vec{m}$) transition dipole moments. The electric (D) and magnetic (G) dipole strengths are defined by the square of electric and magnetic transition dipole moments ($D = |\vec{\mu}|^2$; $G = |\vec{m}|^2$). These parameters for calculating $g_{lum,calcd}$ can be obtained from TD-DFT optimization of the first excited state (S_1). For more detailed information about calculating $g_{lum,calcd}$ we refer to Kubo *et al.*[24]

Table S1. Cartesian coordinates (Å) and transition moments of the optimized structure of *(R_p)*-**1** in the lowest-energy excited state (S_1) calculated at the TD-MN15/def2-TZVP level of theory.

Center Number	Atomic Number	Atomic Type	Coordinates (Angstroms) X	Y	Z
1	6	0	-0.919664	-0.473049	1.887658
2	6	0	-0.933795	0.913158	1.897241
3	6	0	0.128299	1.645617	1.310631
4	6	0	1.297667	0.942730	1.025333
5	6	0	1.326113	-0.464707	1.018281
6	6	0	0.140808	-1.184163	1.295393
7	6	0	-1.326082	-0.464882	-1.017900
8	6	0	-1.297642	0.942607	-1.025226
9	6	0	-0.128187	1.645253	-1.310341
10	6	0	0.933910	0.912548	-1.896899
11	6	0	0.919649	-0.473710	-1.887613
12	6	0	-0.140730	-1.184573	-1.295180
13	6	0	-3.395415	0.253282	-0.249242
14	6	0	-2.640148	-0.898197	-0.557065
15	6	0	-4.696517	0.169732	0.219829
16	6	0	-5.259622	-1.088397	0.388193
17	6	0	-4.528434	-2.237201	0.065091
18	6	0	-3.226682	-2.155903	-0.411655
19	6	0	3.395378	0.253244	0.248994
20	6	0	2.640189	-0.898111	0.557180
21	6	0	4.696366	0.169669	-0.220364
22	6	0	5.259479	-1.088481	-0.388631
23	6	0	4.528374	-2.237184	-0.065134
24	6	0	3.226701	-2.155802	0.411909
25	6	0	0.073793	-2.584994	-0.776119
26	6	0	-0.073892	-2.584723	0.776666
27	6	0	-0.064852	3.039022	0.780623
28	6	0	0.065071	3.038787	-0.780699
29	1	0	-1.811058	-1.017307	2.179285
30	1	0	-1.826316	1.444098	2.208472
31	1	0	1.826460	1.443438	-2.208147
32	1	0	1.810997	-1.017990	-2.179309
33	1	0	-5.245479	1.076178	0.445221
34	1	0	-6.271454	-1.186743	0.760009
35	1	0	-4.990287	-3.209736	0.181689
36	1	0	-2.696130	-3.062084	-0.675045
37	1	0	5.245255	1.076097	-0.446014
38	1	0	6.271236	-1.186876	-0.760633
39	1	0	4.990191	-3.209749	-0.181640
40	1	0	2.696228	-3.061946	0.675591
41	1	0	-0.621561	-3.301279	-1.220030
42	1	0	1.077646	-2.903189	-1.061207
43	1	0	0.621305	-3.301013	1.220805
44	1	0	-1.077822	-2.902691	1.061756
45	1	0	-1.051463	3.401570	1.065914
46	1	0	0.696511	3.707553	1.187881
47	1	0	1.051679	3.401237	-1.066124
48	1	0	-0.696286	3.707220	-1.188134

```
     49          8           0        2.930548    2.628729    0.370872
     50          8           0       -2.930615    2.628759   -0.371456
     51          6           0       -2.587400    1.461138   -0.516243
     52          6           0        2.587412    1.461175    0.516008
---------------------------------------------------------------------
Ground to excited state transition electric dipole moments (Au):
       state          X           Y           Z        Dip. S.      Osc.
         1         0.0016      0.0603      0.0000      0.0036      0.0002
         2        -0.6114     -0.0004     -0.0187      0.3741      0.0258
         3        -0.0055      0.0444     -0.0001      0.0020      0.0001
 Ground to excited state transition velocity dipole moments (Au):
       state          X           Y           Z        Dip. S.      Osc.
         1        -0.0002     -0.0058      0.0000      0.0000      0.0003
         2         0.0670      0.0001      0.0016      0.0045      0.0289
         3         0.0006     -0.0054      0.0000      0.0000      0.0002
 Ground to excited state transition magnetic dipole moments (Au):
       state          X           Y           Z
         1        -0.0022      0.8489     -0.0026
         2         1.1540     -0.0060      1.3049
         3         0.0093      1.0551      0.0121
 Ground to excited state transition velocity quadrupole moments (Au):
       state          XX          YY          ZZ          XY          XZ          YZ
         1         0.5268     -0.0612     -0.1504      0.0001      0.0943      0.0002
         2        -0.0010      0.0006     -0.0003     -0.0157      0.0006     -0.1128
         3         0.2079     -0.0734     -0.0046     -0.0001     -0.0423     -0.0011
 <0|del|b> * <b|rxdel|0> + <0|del|b> * <b|delr+rdel|0>
 Rotatory Strengths (R) in cgs (10**-40 erg-esu-cm/Gauss)
       state          XX          YY          ZZ    R(velocity)    E-M Angle
         1       -17.1613      0.0012    -21.4481    -12.8694      178.36
         2         7.0456    245.6013    290.0354    180.8941       47.15
         3       -20.0443      0.0173    -18.4782    -12.8350      173.02
 1/2[<0|r|b>*<b|rxdel|0> + (<0|rxdel|b>*<b|r|0>)*]
 Rotatory Strengths (R) in cgs (10**-40 erg-esu-cm/Gauss)
       state          XX          YY          ZZ     R(length)
         1         0.0025    -36.2197      0.0000    -12.0724
         2       498.8934     -0.0019     17.2681    172.0532
         3         0.0363    -33.1417      0.0011    -11.0348
  1/2[<0|del|b>*<b|r|0> + (<0|r|b>*<b|del|0>)*] (Au)
       state          X           Y           Z        Dip. S.   Osc.(frdel)
         1        -0.0000     -0.0004      0.0000      0.0004      0.0002
         2        -0.0410     -0.0000     -0.0000      0.0410      0.0273
         3        -0.0000     -0.0002     -0.0000      0.0002      0.0002

 Excitation energies and oscillator strengths:

 Excited State   1:      Singlet-A      2.4743 eV  501.09 nm  f=0.0002  <S**2>=0.000
     108 -> 109       -0.68844
 This state for optimization and/or second-order correction.
 Total Energy, E(TD-HF/TD-DFT) =  -1304.48016542
 Copying the excited state density for this state as the 1-particle RhoCI density.

 Excited State   2:      Singlet-A      2.8149 eV  440.45 nm  f=0.0258  <S**2>=0.000
     103 -> 109       -0.15309
     104 -> 110       -0.11669
     106 -> 110        0.18741
     107 -> 109        0.63805

 Excited State   3:      Singlet-A      2.8558 eV  434.14 nm  f=0.0001  <S**2>=0.000
     103 -> 110        0.34221
     104 -> 109        0.50916
     106 -> 109       -0.25352
     107 -> 110       -0.10306
     108 -> 109       -0.11191
```

7. Cartesian coordinates

(R_p)-1 in DCM

6	0.799274	-0.427738	-1.925187
6	0.805723	0.961027	-1.931824
6	-0.247520	1.685084	-1.357794
6	-1.399539	0.954432	-1.096053
6	-1.417389	-0.452465	-1.101612
6	0.252771	-1.166688	-1.360768
6	1.417265	-0.452640	1.101255
6	1.399365	0.954254	1.095927
6	0.247290	1.684808	1.357696
6	-0.805998	0.960599	1.931437
6	-0.799527	-0.428166	1.924482
6	0.252635	-1.166961	1.360082
6	3.489719	0.221289	0.245182
6	2.729756	-0.906260	0.580618
6	4.764989	0.128346	-0.275236
6	5.304399	-1.143953	-0.465384
6	4.562860	-2.271944	-0.128744
6	3.271283	-2.169104	0.395655
6	-3.489616	0.221223	-0.244811
6	-2.729654	-0.906236	-0.580542
6	-4.764744	0.128140	0.275932
6	-5.303985	-1.144219	0.466155
6	-4.562432	-2.272126	0.129259
6	-3.271008	-2.169140	-0.395489
6	-0.022297	-2.536907	0.786203
6	0.022303	-2.536726	-0.787172
6	-0.016398	3.060738	-0.789961
6	0.016219	3.060602	0.790190
1	1.698964	-0.956564	-2.226332
1	1.704734	1.486887	-2.237734
1	-1.705070	1.486378	2.237302
1	-1.699227	-0.957087	2.225435
1	5.322530	1.022633	-0.528172
1	6.300882	-1.257159	-0.872951
1	4.995422	-3.254273	-0.274520
1	2.724414	-3.066942	0.651212
1	-5.322288	1.022362	0.529086
1	-6.300343	-1.257539	0.873997
1	-4.994867	-3.254502	0.275094
1	-2.724146	-3.066916	-0.651282
1	0.670407	-3.298042	1.148655
1	-1.018232	-2.838712	1.116589
1	-0.670292	-3.297866	-1.149810
1	1.018270	-2.838342	-1.117631
1	0.941482	3.425126	-1.162308
1	-0.791877	3.761278	-1.099764
1	-0.941628	3.424967	1.162625
1	0.791768	3.761008	1.100111
8	-3.015420	2.590473	-0.307656
8	3.015214	2.590494	0.307904
6	2.684279	1.440821	0.525520
6	-2.684357	1.440839	-0.525280

(R_p)-1 in gas phase

6	-0.822350	-0.422743	1.921865
6	-0.825571	0.966159	1.930389
6	0.229699	1.687249	1.358037
6	1.380343	0.954797	1.099850
6	1.398784	-0.450413	1.112159
6	0.232412	-1.162416	1.366812
6	-1.398775	-0.450493	-1.112103
6	-1.380310	0.954717	-1.099883
6	-0.229666	1.687138	-1.358141
6	0.825604	0.965991	-1.930417
6	0.822391	-0.422910	-1.921730
6	-0.232393	-1.162527	-1.366644
6	-3.466980	0.216472	-0.245125
6	-2.711251	-0.907417	-0.596816
6	-4.738839	0.121795	0.279675
6	-5.282193	-1.150202	0.456690
6	-4.547992	-2.275847	0.099109
6	-3.259680	-2.169722	-0.430141
6	3.466986	0.216448	0.245102
6	2.711200	-0.907403	0.596784
6	4.738834	0.121704	-0.279716
6	5.282102	-1.150323	-0.456775
6	4.547831	-2.275932	-0.099224
6	3.259535	-2.169739	0.430051
6	0.036691	-2.531613	-0.786362
6	-0.036689	-2.531551	0.786654
6	0.015161	3.065391	0.790888
6	-0.015146	3.065335	-0.791128
1	-1.728072	-0.948076	2.211138
1	-1.725143	1.493586	2.230701
1	1.725174	1.493388	-2.230780
1	1.728119	-0.948273	-2.210933
1	-5.284990	1.019665	0.542919
1	-6.276650	-1.265861	0.867891
1	-4.984969	-3.258025	0.230877
1	-2.719536	-3.065186	-0.707855
1	5.285035	1.019547	-0.542950
1	6.276545	-1.266035	-0.867997
1	4.984742	-3.258135	-0.231029
1	2.719335	-3.065174	0.707754
1	-0.642495	-3.298228	-1.164204
1	1.040056	-2.829572	-1.098206
1	0.642504	-3.298133	1.164547
1	-1.040046	-2.829486	1.098541
1	-0.937958	3.445605	1.158797
1	0.805606	3.749187	1.099384
1	0.937963	3.445533	-1.159073
1	-0.805610	3.749087	-1.099675
8	2.984079	2.583307	0.269051
8	-2.983886	2.583296	-0.268922
6	-2.660771	1.440832	-0.515384
6	2.660842	1.440847	0.515375

References

[1] G. R. Fulmer, A. J. M Miller, N. H. Sherden, H. E. Gottlieb, A. Nudelman, B. M. Stoltz, J. E. Bercaw, K. I. Goldberg, M. Beckman, *Organometallics,* 2010, **29**, 2176–2179.

[2] M. Tsuchiya, H. Maeda, R. Inoue, Y. Morisaki, R. Li, *Chem. Commun.*, 2021, **57**, 9256–9259.

[3] C. S. Wang, Y. C. Wei, M. L. Pan, C. H. Wu, P. T. Chou, Y. T. Wu, *Chem. Eur. J.,* 2021, **27**, 8678–8683.

[4] E. Lippert, *Ber. Bunsenges. Phys. Chem.,* 1957, **61**, 962–975.

[5] N. Mataga, Y. Kaifu, M. Koizumi, *Bull. Chem. Soc. Jpn*. 1956, **29**, 465–470.

[6] M. Starck, L. E. Mackenzie, A. S. Batsanov, D. Parker, R. Pal, *Chem. Commun.,* 2019, **55**, 14115–14118.

[7], Gaussian 16, Revision C.01, M. J. Frisch, G. W. Trucks, H. B. Schlegel, G. E. Scuseria, M. A. Robb, J. R. Cheeseman, G. Scalmani, V. Barone, G. A. Petersson, H. Nakatsuji, X. Li, M. Caricato, A. V. Marenich, J. Bloino, B. G. Janesko, R. Gomperts, B. Mennucci, H. P. Hratchian, J. V. Ortiz, A. F. Izmaylov, J. L. Sonnenberg, D. Williams-Young, F. Ding, F. Lipparini, F. Egidi, J. Goings, B. Peng, A. Petrone, T. Henderson, D. Ranasinghe, V. G. Zakrzewski, J. Gao, N. Rega, G. Zheng, W. Liang, M. Hada, M. Ehara, K. Toyota, R. Fukuda, J. Hasegawa, M. Ishida, T. Nakajima, Y. Honda, O. Kitao, H. Nakai, T. Vreven, K. Throssell, J. A. Montgomery, Jr., J. E. Peralta, F. Ogliaro, M. J. Bearpark, J. J. Heyd, E. N. Brothers, K. N. Kudin, V. N. Staroverov, T. A. Keith, R. Kobayashi, J. Normand, K. Raghavachari, A. P. Rendell, J. C. Burant, S. S. Iyengar, J. Tomasi, M. Cossi, J. M. Millam, M. Klene, C. Adamo, R. Cammi, J. W. Ochterski, R. L. Martin, K. Morokuma, O. Farkas, J. B. Foresman, and D. J. Fox, Gaussian, Inc., Wallingford CT, 2016.

[8] H. S. Yu, X. He, S. L. Li, D. G. Truhlar, *Chem. Sci.,* 2016, **7**, 5032–5051.

[9] F. Weigend, R. Ahlrichs, *Phys. Chem. Chem. Phys.,* 2005, **7**, 3297–3305.

[10] C. Adamo, D. Jacquemin, *Chem. Soc. Rev.,* 2013, **42**, 845–856.

[11] J. Liu, W. Liang, *J. Chem. Phys.,* 2011, **135**, 184111.

[12] J. Liu, W. Liang, *J. Chem. Phys.* 2011, **135**, 14113.

[13] G. Scalmani, M. J. Frisch, B. Mennucci, J. Tomasi, R. Cammi, V. Barone, *J. Chem. Phys.,* 2006, **124**, 94107.

[14] F. Furche, R. Ahlrichs, *J. Chem. Phys.,* 2002, **117**, 7433–7447.

[15] C. Van Caillie, R. D. Amos, *Chem. Phys. Lett.,* 2000, **317**, 159–164.

[16] C. Van Caillie, R. D. Amos, *Chem. Phys. Lett.,* 1999, **308**, 249–255.

[17] R. E. Stratmann, G. E. Scuseria, M. J. Frisch, *J. Chem. Phys.,* 1998, **109**, 8218–8224.

[18] M. E. Casida, C. Jamorski, K. C. Casida, D. R. Salahub, *J. Chem. Phys.,* 1998, **108**, 4439–4449.

[19] R. Bauernschmitt, R. Ahlrichs, *Chem. Phys. Lett.,* 1996, **256**, 454–464.

[20] A. V. Marenich, C. J. Cramer, D. G. Truhlar, *J. Phys. Chem. B,* 2009, **113**, 6378–6396.

[21] T. Kobayashi, S. Nagakura, *Chem. Phys. Lett.,* 1976, **43**, 429–434.

[22] C. W. Chang, T. I. Sølling, E. W. G. Diau, *Chem. Phys. Lett.,* 2017, **686**, 218–222.

[23] K. Yoshihara, D. R. Kearns, *Chem. Phys.,* 1966, **45**, 1991–1999.

[24] H. Kubo, T. Hirose, T. Nakashima, T. Kawai, J. Y. Hasegawa and K. Matsuda, *J. Phys. Chem.Lett.*, 2021, **12**, 686–695.